Xenotransplantation of Human PSC-derived Microglia Creates a Chimeric Mouse Brain Model that Recapitulates Features of Adult Human Microglia

Ranjie Xu [1], Andrew Boreland [1], Anthony Posyton[1], Kelvin Kwan[1], Ronald P. Hart[1], Peng Jiang[1,*]

[1]Department of Cell Biology and Neuroscience, Rutgers University, Piscataway, NJ 08854, USA.

*Address correspondence to:
Peng Jiang, Ph.D.
Assistant Professor
Department of Cell Biology and Neuroscience
Rutgers University
604 Allison Road, Piscataway, NJ 08854
Email: peng.jiang@rutgers.edu
Phone: 848-445-2805

Abstract

Microglia, the brain-resident macrophages, exhibit highly dynamic functions in neurodevelopment and neurodegeneration. Human microglia possess unique features as compared to mouse microglia, but our understanding of human microglial functions is largely limited by an inability to obtain human microglia under resting, homeostatic states. We developed a human pluripotent stem cell (hPSC)-based microglial chimeric mouse brain model by transplanting hPSC-derived primitive macrophage precursors into neonatal mouse brains. The engrafted human microglia widely disperse in the brain and replace mouse microglia in corpus callosum at 6 months post-transplantation. Single-cell RNA-sequencing of the hPSC microglial chimeric mouse brains reveals that xenografted hPSC-derived microglia largely retain human microglial identity, as they exhibit signature gene expression patterns consistent with physiological human microglia and recapitulate heterogeneity of adult human microglia. Importantly, the chimeric mouse brain also models species-specific transcriptomic differences in the expression of neurological disease-risk genes in microglia. This model will serve as a novel tool to study the role of human microglia in brain development and degeneration.

Introduction

As the resident macrophages of the central nervous system (CNS), microglia play critical roles in maintenance of CNS homeostasis and regulation of a broad range of neuronal responses [1, 2]. Recent studies indicate that dysfunction of microglia contributes to neurodevelopmental and neurodegenerative diseases, including Alzheimer's disease (AD) [3-7]. Moreover, genome-wide association studies have shown that many neurological disease risk genes, particularly many AD risk genes, are highly and sometimes exclusively expressed by microglia [8-10]. These observations provide a compelling incentive to investigate the role of microglia in models of abnormal brain development and neurodegeneration. Most studies of microglia largely rely on rodent microglia. However, there is increasing evidence that rodent microglia are not able to faithfully mirror the biology of human microglia [11]. In particular, recent transcriptomic studies have clearly demonstrated that a number of immune genes, not identified as part of the mouse microglial signature, were abundantly expressed in human microglia [8, 12]. Moreover, a limited overlap was observed in microglial genes regulated during aging and neurodegeneration between mice and humans, indicating that human and mouse microglia age differently under normal and diseased conditions [12, 13]. These findings argue for the development of species-specific research tools to investigate microglial functions in human brain development, aging, and neurodegeneration.

Functional human brain tissue is scarcely available. In addition, given the considerable sensitivity of microglia to environmental changes [8], the properties of available human microglia isolated from surgically resected brain tissue may vary significantly, due to different disease states of the patients and the multi-step procedures used for microglia purification. In order to study human microglia in a relatively homeostatic state, many scientists have turned to human pluripotent stem cells (hPSCs). Recent advances in stem cell technology have led to the efficient generation of microglia from hPSCs [14-19], providing an unlimited source of human microglia to study their function. However, when cultured alone or co-cultured with neurons and astrocytes in 2-dimensional (2D) or 3D organoid/spheroid culture systems, these hPSC-derived microglia best resemble fetal or early postnatal human microglia, as indicated by much lower expression of key microglial molecules such as TREM2, TMEM119, and P2RY12 in the hPSC-derived microglia, as compared to microglia derived from adult human brain tissue [16, 18, 20]. Thus, even with these novel *in vitro* models, it has been challenging to advance understanding of human microglial function in adult ages or in neurodegeneration during aging.

Recent studies from us [21, 22] and others [23-25] have demonstrated that neonatally engrafted human neural or macroglial (oligodendroglial and astroglial) progenitor cells can largely repopulate and functionally integrate into the adult host rodent brain or spinal cord, generating widespread chimerism. This human-mouse chimeric approach provides unique opportunities for studying the pathophysiology of the human cells within an intact brain. In this study, we developed a hPSC microglial chimeric mouse brain model, by transplanting hPSC-derived microglia into neonatal mouse brains. The engrafted hPSC-derived microglia can proliferate, migrate, and widely disperse in the brain. We hypothesize that the limited functional maturation of hPSC-derived microglia in *in vitro* models is primarily caused by the fact that those microglia are maintained in an environment that lacks the complex cell-cell/cell-matrix interactions existing in an *in vivo* brain environment [8]. To test this hypothesis, we employed single-cell RNA-sequencing to examine the gene expression profile of hPSC-derived microglia developed for six months in the mouse brain.

Results

Generation of hPSC microglial chimeric mouse brains

Microglia originate from yolk sac erythromyeloid progenitors (EMPs) during primitive hematopoiesis. EMPs further develop to primitive macrophage precursors (PMPs) that migrate into the developing neural tube and become microglia with ramified processes within the CNS environment [1]. We first derived PMPs from hPSCs, including one human induced pluripotent stem cell (hiPSC) line and one human embryonic stem cell (hESC) line, using a published protocol [18]. Briefly, the yolk sac embryoid bodies (YS-EBs) were generated by treating the EBs with bone morphogenetic protein 4 (BMP4), vascular endothelial growth factor (VEGF), and stem cell factor (SCF). Next, the YS-EBs were plated into dishes with interleukin-3 (IL-3) and macrophage colony-stimulating factor (M-CSF) to promote myeloid differentiation. At 2–3 weeks after plating, hPSC-derived hPMPs emerged into the supernatant and were continuously produced for more than 3 months. The cumulative yield of PMPs was around 40-fold higher than the number of input hPSCs (Figure 1A), similar to the results from previous studies [16, 18]. PMPs are produced in a Myb-independent manner that closely recapitulated primitive hematopoiesis [1]. We confirmed the identity of these hPSC-derived PMPs by staining with CD235, a marker for YS primitive hematopoietic progenitors [26, 27], and CD43, a marker for hematopoietic progenitor-like cells[26, 27]. As shown in Figure 1B, over 95% of the hPSC-derived PMPs expressed both markers. Moreover, the human PMPs are highly proliferative as indicated by Ki67 staining (95.4 ± 2.2%, n = 4) (Figure 1B). Using this method, we routinely obtain ample numbers of hPSC-derived PMPs with high purity as required for cell transplantation experiments.

We engrafted hPSC-derived PMPs into the brains of postnatal day 0 (P0) immunodeficient mice that are Rag2/IL2rγ-deficient and also express the human forms of CSF1, which facilitates the survival of xenografted human myeloid cells and other leukocytes. We deposited cells into the white matter overlying the hippocampus and sites within the hippocampal formation (Figure 1C). In order to visualize the distribution of donor-derived microglia, at 6 months post-transplantation, we stained the mouse brain sections with human-specific antibody recognizing TMEM119 (hTMEM119). TMEM119 is a marker that is only expressed by microglia, but not other macrophages [14, 17, 28]. We found that the donor-derived hTMEM119$^+$ microglia migrated long distances along the corpus callosum to reach the olfactory bulb (Figure 1D). The is consistent with the observation in the developing brain that microglia use white matter tracts as guiding structures for migration and that they enter different brain regions [29]. As early as 3 weeks post-transplantation, donor-derived microglia had already migrated along corpus callosum and passed through the rostral migratory stream to the olfactory bulb (Figure 1E). At 6 months post-transplantation, human microglia widely dispersed in multiple brain regions, including olfactory bulb, hippocampus, and cerebral cortex, and exhibited a highly ramified morphology (Figure 1F and G) typical of resting microglia. Similar to our previous studies [24, 25], we assessed the engraftment efficiency and degree of chimerization by quantifying the percentage of hTMEM119$^+$ cells among total DAPI$^+$ cells in the forebrain in sagittal brain sections covering regions from 0.3 to 2.4 mm lateral to midline and found that about 8% of the total cells were human microglia in the 6-month-old mouse brains (Figure 1D and L). Frequently, we also observed clusters of human microglia in the cerebellum (Figure 1H), which might be a result from the strong ability of immune cells trafficking along blood vessels and/or the choroid plexus [30]. These results demonstrate that hPSC-derived PMPs survive in mouse brain and that they migrate to a variety of structures.

To examine whether transplanted hPSC-derived PMPs efficiently differentiated to microglia in the mouse brain, we double-stained brain sections for both human nuclei (hN) and hTMEM119. As early as 8 weeks post-transplantation, the vast majority of hN$^+$ PMPs (92.3 ± 1.5%, n =10) were positive for hTMEM119 (Figure 1I and M), indicating the robust and efficient differentiation of hPSC-derived PMPs into microglia. Moreover, the vast majority of the donor-derived cells expressed PU.1, a transcription factor that is necessary for microglial differentiation and maintenance[31-34], and were positive for human specific CD45 (hCD45), which is expressed by all nucleated hematopoietic cells [35, 36]. Furthermore, we assessed the proliferation of engrafted cells by staining the proliferative marker Ki67. As shown in Figure 1K and N, at 3 weeks post-transplantation, about 17% (16.9 ± 5.7%, n = 8) of

hN$^+$ transplanted cells expressed Ki67, indicating that these cells were capable of proliferating in the mouse brain. At 6 months post-transplantation, the percentage of proliferating cells dramatically decreased and less than 2% (1.7 ± 0.8%, n = 7) of total engrafted cells were Ki67 positive. These Ki67$^+$ proliferating human cells mainly localized in the subventricular zone, the walls along lateral ventricles, corpus callosum, and olfactory bulb (Figure 1K and supplementary Figure 1B). Taken together, these findings demonstrate that engrafted hPSC-derive PMPs differentiate to microglia, generating a mouse brain with a high degree of human microglial chimerism in the forebrain.

Human PSC-derived microglia undergo morphological maturation and are functional in the mouse brain

Compared with three weeks post-transplantation, hPSCs-derived microglia appeared to exhibit more complex processes at 6 months post-transplantation (Figure 1E and F). Moreover, even at the same stage, hPSC-derived microglia in the cerebral cortex seemed to exhibit much more complex morphology, compared with the hPSCs-derived microglia in the corpus callosum and cerebellum (Figure 1G and H, supplementary Figure 1B and 2A). In the corpus callosum, hPSC-derived microglia had fewer branches that aligned with axons; and in the cerebral cortex, the microglia exhibited more complex and ramified processes (supplementary Figure 1B and 2A), similar to the observation from previous studies [29, 37]. This prompted us to further examine the morphological and functional changes of the hPSC-derived microglia along with the development of the mouse brain, particularly in cerebral cortex. Previous studies have shown that there are not changes in microglial number, cytokine levels, and gene expression profiles between wild type and *Rag2*$^{-/-}$ mice [38]. Building upon that, we also compared the differences between xenografted hPSC-derived microglia vs. host mouse microglia. We double-stained the brain sections with human and mouse specific TMEM119 (hTMEM119 and mTMEM119, respectively) antibodies to distinguish hPSC-derived microglia and mouse host microglia. As shown in Figure 2A, in 6 months old mice, both hPSCs-derived microglia and mouse microglia were seen in the cerebral cortex and hippocampus. Notably, hPSCs-derived microglia seemed to expel mouse microglia, as indicated by the observation that mouse microglia mainly resided in distal regions in the cerebral cortex and hippocampus. Particularly, in the corpus callosum, mouse microglia were rarely seen, and the vast majority of microglia were hPSC-derived microglia, indicating that hPSC-derived microglia replaced the host mouse microglia. In the cerebral cortex, hTMEM119$^+$ hPSC-derived microglia exhibited much more complex processes at 8 weeks and 6 months post-transplantation than those cells at 3 weeks post-transplantation, as indicated by the increased number of endpoints (Figure 2C). The total length of processes of hPSC-derived microglia also significantly increased from week 3 to week 8 and month 6 (Figure 2D), suggesting the gradual maturation of hPSC-derived microglia in mouse brain. We further examined the morphological differences between hPSC-derived microglia vs. mouse microglia at the same time points after transplantation. In the cerebral cortex, at 3 weeks post transplantation, compared with hPSC-derived microglia, mouse microglia showed a significantly higher number of endpoints and a slight trend of longer processes (Figure 2C and 2D). However, at 8 weeks post-transplantation, there was no significant difference in endpoint number and process length between hPSC-derived microglia and mouse microglia (Figure 2C and 2D). Interesting, at 6 months post-transplantation, hPSC-derived microglia exhibited a significantly higher number of endpoints and longer process length than mouse microglia. Since microglial morphology is inextricably linked to their phagocytic functions [39, 40], we examined the expression of CD68, a lysosomal marker indicative of the phagocytic activity of microglia [41]. In the cerebral cortex, CD68 was expressed in vast majority of the hPSC-derived microglia at 3 weeks post-transplantation (33.9 ± 3.7%) and its expression dramatically decreased from 8 weeks to 6 months post-transplantation (Figure 2G and E). We observed some hTMEM119$^-$/CD68$^+$ cells at 3 weeks and nearly no hTMEM119$^-$/CD68$^+$ cells at 6 months post-transplantation (Figure 2G), suggesting that nearly no host mouse microglia expressed CD8 at 6 months post-transplantation. Microglia have been shown to shape synapse formation by pruning synapses and to maintain oligodendroglial homeostasis, by phagocytizing oligodendroglial cells [42-44]. We then investigated whether hPSCs-derived microglia were also able to prune synapse in the mouse

brain. By double staining human microglia marker hCD45 with a synapse marker PSD95, we found that some PSD95$^+$ puncta localized inside of the hCD45$^+$ processes of hPSC-derived microglia. This engulfment of synaptic materials was observed from 3 weeks to 6 months post-transplantation, most prominently seen at 8 weeks post-transplantation, diminishing to only a few at 6 months (Figure 2G and F). By double staining hCD45 with oligodendroglial marker Olig2, we found that hPSCs-derived microglia in white matter clearly engulfed Olig2$^+$ oligodendroglia at 3 weeks post-transplantation (supplementary Figure 2B). Microglia, together with endothelial cells, pericytes and astrocytes, form the functional blood–brain barrier. We double-stained the brain sections with hCD45 and laminin, a marker that has been commonly used to visualize vascular structures in the mammalian brain [45]. We found that hPSC-derived microglia clustered around and were closely affiliated with blood vessels in both grey matter and white matter across different brain regions including the olfactory bulb (Figure 2H and supplementary Figure 2C). Taken together, hPSC-derived microglia show variable morphologies in a spatiotemporal manner, morphologically differ from the host mouse microglia, and are functional in mouse brain.

Single-cell RNA-sequencing of hiPSC microglial chimeric mouse brain identifies a gene expression signature consistent with adult human microglia

Homeostatic human microglia at adult stages are difficult to obtain, because microglia are highly sensitive to environmental changes and microglia derived from adult human brain tissue-derived are usually purified through multi-step procedures that can change their biological properties significantly [8]. In addition, microglia derived from hPSCs using all current differentiation protocols largely resemble fetal or early postnatal human microglia[16, 18, 20]. We hypothesize that hPSC microglial chimeric mice may provide a unique opportunity to study biological properties of adult human microglia, because the engrafted hPSC-derived microglia are likely to exhibit an expedited maturation process promoted by the maturing environment in the mouse brain. To test this hypothesis, we examined transcriptomic profiles of hiPSC-derived microglia developed in the *in vivo* homeostatic mouse environment using single-cell RNA-sequencing (scRNA-seq). We collected brain regions where engrafted hiPSCs-derived microglia preferentially dispersed, including the cerebral cortex, hippocampus, corpus callosum, and olfactory bulb, from 6-month-old chimeric mouse brain for scRNA-seq. Owing to the wide distribution and high abundance of hiPSC-derived microglia in those brain regions, we were able to capture ample number of hiPSC-derived microglia for scRNA-seq without using FACS sorting, which has the potential to impact transcriptional profiles through extended ex vivo manipulation. After brain tissue dissociation with papain and centrifugation to remove debris and myelin, single cell suspensions were directly subjected to droplet-based 10X Genomic RNA-seq isolation (Fig. 3A). Using stringent criteria, 29,974 cells passed the quality control evaluation (with about 10,000–15,000 reads/cell) from 4 animals for downstream analysis (Fig. S3A).

We performed dimensionality reduction and clustering using a principal component analysis (PCA)-based approach. Using t-distributed stochastic neighbor embedding (t-SNE) to visualize cell clustering, we identified 11 clusters, including a cluster of xenografted hiPSC-derived microglia, which we named Xeno MG (Fig. 3B). This clustering pattern was consistently seen in all four animals, indicating the high reproducibility of the sequencing and clustering procedures (Fig. S3B). We defined each cluster based on the expression of enriched genes (Table S1) that could be recognized as markers for specific cell types or are reported to be abundantly expressed in specific cell types (Figure 3C and Figure S3C). The clusters included 10 mouse cell types: astrocytes (*SCL6A11*[46], *NTSR2*[47]), oligodendrocytes (*CLDN11*[48], *CNP*[49]), oligodendrocyte progenitor cells (OPC; *PDGFRα*, *OLIG2*[50]), excitatory neurons (*SYT1*[51], *SNAP25*[52]), neuronal precursors (*SOX11*, [53], *STMN2*, [54]), vascular cells (*MYL9*[55], *MGP*[56]), choroid cells (*LCN2*[57],*1500015O10Rik*[58]), endothelial cells (*ITM2A*[59], *FLT1*[60]), GABAergic neuron (*NPY*[61], *NR2F2*[62]) and mouse microglia (*CTSS, HEXB*[8]). The only human cell cluster, labeled Xeno MG, preferentially expressed the microglial markers *SPP1* and *CD74*, and accounted for about 7% of total cells (Figure S3D). Of note, a cross-correlation analysis of clustered cell types showed that Xeno MG had a highest correlation coefficient value (0.765) with mouse

microglia, consistent with a microglial identity of the engrafted human cells (Figure S3E). Furthermore, the expression of a set of canonical microglial genes (*C1QA*, *CX3CR*, *TREM2*, *CSFRR*, and *P2RY12*) was only detected in Xeno MG and mouse microglia clusters (Figure 3D). We examined the expression of the top 30 human microglial signature genes reported by a previous study [8]. We found that the vast majority of human microglia signature genes were exclusively or abundantly expressed in Xeno MG, as compared to the other types of cells in chimeric mouse brains (Figure 3E). Furthermore, we compared the transcriptomic profile of Xeno MG with a published dataset generated from human brain tissue-derived human microglia[12]. A significant correlation was observed between Xeno MG and the published dataset[12] (Figure S4A), further confirming the human microglial identity of the engrafted human cells. As shown in Figures 1 and 2, the highly ramified morphology of hiPSC-derived microglia strongly indicate that they exhibit a quiescent and non-activated state. To confirm this, we examined expression of several pro-inflammatory cytokines to assess the impact of the tissue preparation procedures on the microglial state. We found very minor expression of acute pro-inflammatory cytokines such as IL-1β, IL-1α and TNF-α[63 64, 65] (Figure S4B). In contrast, the pro-inflammatory cytokine, IL-6 and an anti-inflammatory cytokine, IL-10, were nearly undetectable, and expression of these pro-inflammatory cytokines is often correlated with a longer-lasting inflammatory response[64, 65]. This observation suggests that only a very mild inflammatory reaction was likely triggered in the Xeno MG during sample preparation, similar to previous reports [44, 63]. These results demonstrate that Xeno MG developed in the mouse brain largely retain their human microglial identity and exhibit a gene expression pattern characteristic of physiologically normal human microglia.

Next, to explore the maturation of Xeno MG in chimeric mouse brains, we compared the global expression patterns of 547 genes which were previously identified as aging-regulated genes using human microglia derived from individuals ranging from ages 34 to 102 [12], between our Xeno MG and published datasets of hiPSC-derived microglia cultured under 2-dimensional (2D) conditions (iPS MG)[17, 66], hiPSC-derived microglia developed in 3D cerebral organoids (oMG)[67] , brain-tissue derived adult human microglia (adult MG) [12, 67], as well as blood/liver macrophages[17, 66]. As shown in Figure 3F, a principal component analysis (PCA) demonstrated that Xeno MG were markedly distinct from blood/liver macrophages. Evaluating maturity, the iPS MG cultured under 2D conditions most resembled fetal microglia, which is consistent with previous reports [14, 16]. The oMG developed in organoids showed more mature characteristics, intermediate between fetal and adult microglia along the first principal component, but still quite distinct from the cluster of adult MG. Remarkably, our Xeno MG clusters intermingled with a cluster of adult MG samples, indicating their resemblance to adult human microglia (Figure 3F). Recent unbiased hierarchical clustering analyses revealed four major subclasses of adult human microglia derived from human brain tissue [68]. To determine if Xeno MG also exhibited similar heterogeneity in chimeric mouse brain, we examined the expression of the most differentially regulated genes identified from the different subclasses of adult human microglia [68]. Gene expression analysis revealed that *CD74*, *SPP1*, *C3*, and *CST3*, which were highly expressed in all subclasses in adult human microglia, had a similarly uniform pattern of expression among most Xeno MG cells. Moreover, a chemokine gene *CCL4*, the zinc finger transcription factors *EGR1*, *EGR2* and *EGR3*, *CD83*, and *MCL1*, which are each characteristically expressed in individual subclasses of human microglia, similarly had upregulated expression in distinct subpopulations of Xeno MG (Figure 3G, Figure S4C). Taken together, these results demonstrate that Xeno MG developed in the mouse brain highly resemble adult human microglia and faithfully recapitulate heterogeneity of adult human microglia.

Transcriptomic profiling analysis reveals differences between co-resident Xeno MG and mouse microglia

Previous studies reported differences in transcriptomic profiles between human and mouse microglia [8, 12]. In the chimeric mouse brain, as xenografted hiPSC-derived microglia and host mouse microglia developed in the same brain environment, this model may provide a unique opportunity to directly examine the differences between human and mouse microglia. Xeno MG and host mouse microglia

clusters obtained from 4 independent samples of 6-month-old chimeric mouse brains were used for the following comparison (Figure 4A). We first compared the average levels of microglial gene transcripts in Xeno MG with orthologous gene transcripts in host mouse microglia. Consistent with previous findings [8, 12], the comparison between Xeno MG and mouse microglial transcriptomes demonstrated similar gene expression patterns overall ($r^2 = 0.553$; $p < 2.2 \times 10^{-16}$), and the majority of orthologous genes pairs (14,488 of 15,058; 96.2%) were expressed within a twofold range (Figure 4B). Using a cut-off of 2-fold difference and an FDR of 0.05, we identified that 248 gene transcripts were preferentially expressed in human microglia, whereas 247 gene transcripts were preferentially expressed in mouse microglia (Figure 4D, Table S2). Importantly, previously-reported signature genes expressed in human microglia[8], including *SPPI*, *A2M*, and *C3*, and signature genes expressed in mouse microglia, including *HEXB*, *SPARC*, and *SERINC3*, were all differentially expressed in our sequencing data (Figure 4B and C), indicating the high fidelity of our samples in resembling previously-identified human vs. mouse microglial gene expression profiles. To explore the function of genes that were highly expressed human microglia, we further performed Gene Ontology (GO) term analysis. Many significantly enriched terms were associated with the innate immune activity of microglia, such as “immune system response,” “regulation of immune system process response,” and “leukocyte activation,” which is consistent with a recent study [12, 69]. In addition, we observed enrichment of genes associated with “regulation of cell adhesion,” “cytoplasmic translation,” and “peptide biosynthetic process” (Figure 4E). These results suggest that compared to the host mouse microglia, Xeno MG may be more immunocompetent, as they express an enriched set of immune receptors and ligands.

Previous studies have shown that several disease risk genes, such as genes associated with AD, Parkinson’s disease (PD), multiple sclerosis (MS), and schizophrenia (SCZ), are preferentially expressed in microglia[8, 69, 70]. Moreover, relative expression of these genes in human and mouse microglia are also different [8]. Therefore, we examined the expression of disease risk genes in Xeno MG and mouse microglia from our chimeric mouse brain preparation. Expression of disease risk genes, as reported in a recent study [8], had a highly similar differential expression pattern in co-resident mouse and human microglia (Figure 4F, G and Figure S4D, S4E). Specifically, with respect to AD, we found that out of 14 AD genes, 10 genes, including *Apoc1, Sorl2,* and *Mpzl1,* were more abundantly expressed in Xeno MG than in mouse microglia (Figure 4F and H). Similarly, out of the 20 PD genes listed in a previous report [8], 18 genes, such as *Vps13c, Snca, Fgf20, Mnnrn1*, and *Lrrk2*, had the same trend of differential expression with greater expression in Xeno MG than in mouse microglia (Figure 4G and H). We also found that some of the disease genes were preferentially expressed in mouse microglia, such as *Syt11*and *Gba* in PD. Altogether, these observations demonstrate that our hPSC microglial chimeric mouse brain can faithfully model the transcriptomic differences between human and mouse microglia, and this new model will serve as a new tool for modeling human neurological disorders that involve dysfunction of microglia.

Discussion

Humanized mouse models, in which the immune system is reconstituted by cells of human origin, have been well-established and provide powerful tools for studying cancer, inflammatory and infectious disease, and human hematopoiesis [71]. However, there are no previous studies reporting a mouse model in which the brain is largely repopulated by human brain-resident immune cells, microglia. In this study, by engrafting neonatal mice with hPSC-derived PMPs, we demonstrate the generation of chimeric mouse brains in which hPSC-derived microglia widely disperse. We propose that the following three reasons may account for the generation of human microglial chimeric mouse brain. First, as compared to other types of neural cells, microglial cells are unique in that they turn over remarkably quickly, allowing the vast majority of the population to be renewed several times during a lifetime [72-74]. Previous studies have shown that neonatally transplanted human macroglial or neural progenitor cells can outcompete and largely replace the host mouse brain cells [21, 22, 75]. In this study, we also observe that the hPSC-derived PMPs are highly proliferative prior to transplantation and transplanted cells divide for at least 6 months in the mouse host brain. Therefore, the nature of high turnover rate of microglia and the competitive advantage of engrafted human cells over endogenous mouse cells may result in a large number of human donor-derived microglia and brain regions being repopulated by hPSC-derived microglia in the mouse brain at 6 months. Second, during early brain development, microglial cells use blood vessels and white matter tracts as guiding structures for migration and enter all brain regions [29]. Thus, transplantation of hPSC-derived PMPs to the anterior anlagen of the corpus callosum of the neonatal mouse brain in this study may facilitate migration of donor cell-derived microglia, resulting in wide dispersion of hPSC-derived microglia into different brain regions. In addition, in support of this concept, we also observe that in the mouse brain, hPSC-derived microglia are concentrated around and have close contact with blood vessels in both grey matter and white matter. Lastly, although previous studies have also transplanted hPSC-derived microglia into mouse brains, the generation of chimeric mice with a high degree of human microglial brain chimerism has not been reported [16, 76]. We propose that this might be because of the age of the host animals used for cell transplantation. Previous studies used adult animals for cell transplantation [16, 76]. In our study, we transplanted hPSC-derived PMPs into the mouse brain at the earliest postnatal age, P0, as in general the neonatal brain is more receptive for the transplanted cells and more conducive for their survival and growth [21, 22, 24]. Moreover, in contrast to studies that examined donor-derived microglia 2 months after transplantation, we characterized the donor-derived microglia up to 6 months post-transplant, which allowed the donor cells to develop for a longer term in the mouse brain.

Remarkably, the single-cell sequencing analysis demonstrates that xenografted hiPSC-derived microglia developed in the mouse brain retain a human microglial identity, as indicated by exhibiting a human microglia-specific transcriptomic signature. More importantly, xenografted hiPSC-derived microglia showed expression patterns of microglial maturity resembling adult human microglia derived from human brain tissue. Therefore, establishment of such a hiPSC microglial chimeric mouse model provides novel opportunities for understanding the biology of human microglia. First, this proof-of-concept study paves the path to interrogating the species differences between human vs. mouse microglia at molecular, functional, and behavioral levels using this hiPSC microglia chimeric mouse brain model. It has been increasingly recognized that as compared to mouse microglia, human microglia possess unique features under conditions of development, aging and disease [8, 11-13]. In our model, human and mouse microglia develop in the same brain, but we have observed that human microglia are morphologically distinct from their mouse counterparts and also exhibit signature gene expression profiles characteristic of human microglia isolated from brain. Microglia are intimately involved in processes of neuronal development, such as neurogenesis, synaptogenesis, and synaptic pruning [77-79]. Building upon the differential expression profiles, our model will be useful to investigate how human and mouse microglia function differently in shaping neuronal development. Moreover, this hiPSC microglial chimeric mouse model will provide unprecedented opportunities to understand how the inclusion of human microglia in the developing brain ultimately impacts behavioral performance of

the animals. Second, several transcriptomic studies [12, 20] have clearly demonstrated that microglial genes are differently regulated during aging and neurodegeneration between mice and humans, indicating the importance of developing a human microglia model to study human microglial function across different development stages, particularly adult microglia for studying aging-related and neurodegenerative disorders. PCA analysis of aging-regulated genes demonstrates that in contrast to hiPSC-derived cultured under 2D or 3D organoid conditions, xenografted hiPSC-derived microglia were indistinguishable from adult human microglia. Combining this with human iPSC technologies, such as the availability of edited, isogenic cells with or without disease-related genes, the hiPSC microglia chimeric mouse model will be informative in teasing out the roles of human microglia in neurodevelopmental disorders, neurodegenerative disorders, as well as brain infections by viruses such as Zika virus and HIV-1.

Similar to reports of hiPSC macroglial or neuronal chimeric mouse brain models [21, 22, 24], in the current hPSC microglial chimeric mouse model, the endogenous mouse counterpart cells are still present. In contrast to macroglial cells and neurons, microglial cells can be acutely depleted (up to 99% depletion) in the entire brain without significantly affecting the viability of animals, by pharmacologically inhibiting signaling pathways that are important for the survival and development of microglia, such as colony-stimulating factor 1 (CSF1) signaling [80] or by genetically coupling suicide genes under the control of promoters of microglia-specific genes [1, 81]. In future studies, it will be interesting to explore the possibility of creating humanized mouse brains containing solely hiPSC-derived microglia, by depleting endogenous mouse microglia using pharmacological or genetic approaches in neonatal mouse brains prior to engraftment of hiPSC-derived microglia. In addition, co-transplantation of human PSC-derived PMPs and neural or macroglial progenitors may generate chimeric mouse brain containing human microglia, neurons, and macroglial cells. Currently, in this proof-of-concept hPSC microglial chimeric mouse brain model, there is a lack of peripheral adaptive immune system in the host due to a *Rag2*$^{-/-}$ mutation. To circumvent this limitation, hiPSC-derived PMPs can be transplanted into animals in which the immune system is humanized by the same hiPSC-derived hematopoietic stem cells [32, 82, 83]. This will further allow the generation of animals with isogenic adaptive immune system and brain innate immune system derived from the same human individuals. Combined with recently developed hiPSC cerebral organoid models that contain microglia [16, 67], chimeric mouse brain models may help further our understanding of the complex interactions between human microglia and human neurons and macroglial cells under normal and disease conditions.

METHOD DETAILS

Generation, culture, and quality control of hPSC lines.

One healthy control hiPSC line and H9 ESC line were used this study. The hiPSC line were generated from healthy person-derived fibroblasts using the "Yamanaka" reprogramming factors, as reported in our previous study [84] . The hiPSC line has been fully characterized by performing karyotyping, teratoma assay, DNA fingerprinting STR (short tandem repeat) analysis, gene expression profiling, and Pluritest (www.PluriTest.org), a robust open-access bioinformatic assay of pluripotency in human cells based on their gene expression profiles [85], as described in our previous study [84]. The hPSCs were maintained under feeder-free condition and cultured on dishes coated with hESC-qualified Matrigel (Corning) in mTeSR1 media (STEMCELL Technologies). The hPSCs were passaged approximately once per week with ReLeSR media (STEMCELL Technologies). All the hPSC studies were approved by the committees on stem cell research at Rutgers University.

PMP generation and culture

PMP were generated from hiPSCs and H9 hESCs, using a published protocol [18]. Briefly, the yolk sac embryoid bodies (YS-EBs) were generated by treating the EBs with bone morphogenetic protein 4 (BMP4, 50 ng/ml, Peprotech; to induce mesoderm), vascular endothelial growth factor (VEGF, 50 ng/ml, Peprotech; endothelial precursors), and stem cell factor (SCF, 20 ng/ml, Miltenyi Biotech; hematopoietic precursors). Next, the YS-EBs were plated into dishes with interleukin-3 (IL-3, 25 ng/ml, Peprotech) and macrophage colony-stimulating factor (M-CSF, 100 ng/ml, Invitrogen) to promote myeloid differentiation. At 2–3 weeks after plating, human hPMPs emerged into the supernatant and were continuously produced for more than 3 months. The cumulative yield of PMPs was around 40-fold higher than the number of input hPSCs (Figure 1A), similar to the previous studies [16, 18]. PMPs were produced in a Myb-independent manner and closely recapitulating primitive hematopoiesis [1].

Animals and Cell transplantation

PMP were collected from supernatant and suspended as single cells at a final concentration of 100,000 cells per µl in PBS. The cells were then injected into the brains of P0 Rag2$^{-/-}$hCSF1 immunodeficient mice (C;129S4-*Rag2*$^{tm1.1Flv}$ *Csf1tm1*$^{(CSF1)Flv}$ *Il2rg*$^{tm1.1Flv}$/J, The Jackson Laboratory). The precise transplantation sites were bilateral from the midline = ± 1.0 mm, posterior bregma = -2.0 mm, and dorsoventral depth = -1.5 and -1.2 mm (Figure 1C). The mouse pups were anesthetized by placing them on ice for 5 minutes. Once cryo-anesthetized, the pups were placed on a digital stereotaxic device (David KOPF Instruments), equipped with a neonatal mouse adaptor (Stoelting). The pups were then injected with 0.5 µl of cells into each site (total 4 sites) by directly inserting Hamilton needles through the skull into the target sites. The pups were weaned at 3 weeks and were kept up to 6 months before they were tested for the engraftment of human cells. All animal work was performed without gender bias under the Institutional Animal Care and Use Committee (IACUC) protocol approved by Rutgers University IACUC Committee.

Sample preparation and library construction for Single-cell RNA sequencing

Six months old chimeric mice that received transplantation of microglia derived from the hiPSC line were used for single-cell RNA-sequencing experiments. The mice were perfused with oxygenated solution (2.5 mM KCl, 87 mM NaCl, 1.25 mM NaH_2PO_4, 26 mM $NaHCO_3$, 75 mM sucrose, 20 mM glucose, 2 mM $MgSO_4$, and1 mM $CaCl_2$) as reported [86] and the brain was quickly extracted and kept in the same cold solution for vibratome (VT1200, Leica) sectioning (500µm thickness) and dissection. The brain regions were isolated from where engrafted hiPSCs-derived microglia largely dispersed, including the cerebral cortex, hippocampus, corpus callosum, and olfactory bulb. The selected regions were chopped with Spring Scissors (WPI) into fine pieces for further dissociation into single cells, based on 10x Genomic Sample Preparation Domstratd Protocol (Dissociation of Mouse Embryonic Neural Tissue) with modifications. Briefly, the pieces were collected and dissociated with the Papain (1mg/ml,

Sigma) and DNAase I (100 unit/ml, Roche) in Hibernate solution (Gibco) in 37℃ for 20 minutes. Tissues were washed and triturated with wide-bore tips in cold Hibernate solution until no visible chunks. The samples were spun down in 200 rcf for 2 minutes in 4℃ and filtered through 30 μm cell strainer to obtain single cells for cell counting and library preparation. To generate libraries, 20,000 cells were loaded for each sample. cDNA libraries were generated following the manufacturer instructions.

Single-cell RNA sequencing

Single cell RNA sequencing was performed by RUCDR® Infinite Biologics at Rutgers by using a 10X Genomics single cell gene expression profiling kit. The libraries were analyzed on Agilent 4200 TapeStation System using High Sensitivity D1000 ScreenTape Assay (Cat #: 5067-5584) and quantified using KAPA qPCR (Cat # KK4835). Libraries and then normalized to 10nM before being pooled together. The pooled library was then clustered and sequenced on Illumina HiSeq 2500 in Rapid Run Mode, using the following parameters: 36bp forward read, 100bp reverse read, and 8bp index read. For each individual library, the sequencing data from 4 unique indexes were combined before further analysis.

Sequencing reads were aligned with pooled mouse (mm10) and human (hg19) reference genomes and the barcodes were interpreted using Cellranger software (10X Genomics, v. 3.0.0). The resulting matrices of gene counts x barcodes were coded by individual sample identifier and loaded into Seurat (v. 2.3.4) software [87-89] in R/Bioconductor [90]. An initial analysis revealed a distinct cluster of human-expressing cells. To compare expression across species, a strategy was employed similar to one used previously [91]. A table of 17,629 unique matching genes was prepared, starting with a human-mouse gene homology list obtained from Jackson Labs (http://www.informatics.jax.org/downloads/reports/index.html#marker), and hand-curating to remove duplicates (Table S3). Sample/barcode identifiers for the human-specific data were isolated and matching gene symbols were converted from human to mouse. Sample/barcode identifiers not matching this cluster were assumed to be mouse, and these were trimmed to retain only mouse gene symbols matching the homology list. The resulting tables were merged for subsequent analysis in Seurat.

For comparisons among sources of human microglia, raw RNAseq reads from the human-specific cluster were pooled by sample and aligned with reference human genome (hg38) using HISAT2 [92]. Raw sequencing reads from other publications were downloaded from GEO (series accessions GSE99074[12], GSE97744[17], and GSE102335[67]). Since most of these used a different single-cell sequencing technology which produced larger numbers of reads (~80M vs. an average of 8M from each pooled human microglial sample), we randomly down-sampled sequencing reads to about 10% prior to analysis to prevent inflation of the shallower-read samples upon normalization. After similar HISAT2 alignment, all count summaries were imported into a DESeq2 [93] data model. Expression data were filtered for genes identified as regulated in human microglia over aging, including 212 up-regulated and 360 down-regulated genes [12], and then summarized by principal components analysis in R.

For analysis of human microglial sub-clusters, extracted human sample/barcode were restricted to human gene symbol results and re-analyzed with Seurat. Gene ontology analysis used the g:Profiler [94] website (https://biit.cs.ut.ee/gprofiler/gost) with lists of gene symbols listed in Supplementary Table 2.

Immunostaining and cell counting

Mouse brains fixed with 4% paraformaldehyde were processed and cryo-sectioned for immunofluorescence staining [95, 96]. The primary antibodies were listed in supplementary Table 4. Slides were mounted with the anti-fade Fluoromount-G medium containing 1, 40,6-diamidino-2-phenylindole dihydrochloride (DAPI) (Southern Biotechnology). Images were captured with Zeiss 710 confocal microscope. The analysis of fluorescence intensity was performed using ImageJ software (NIH Image). The relative fluorescence intensity was presented as normalized value to the control group. The cells were counted with ImageJ software. For brain sections, at least five consecutive sections of each brain

region were chosen. The number of positive cells from each section was counted after a Z projection and at least 7 mice in each group were counted. Engraftment efficiency and degree of chimerization were assessed by quantifying the percentage of hN^+ cells among total $DAPI^+$ cells in sagittal brain sections, as reported in the previous studies [24, 25]. The cell counting was performed on every fifteenth sagittal brain section with a distance of 300 μm, covering brain regions from 0.3 to 2.4 mm lateral to the midline (seven to eight sections from each mouse brain were used).

Data analysis

All data represent mean ± s.e.m. When only two independent groups were compared, significance was determined by two-tailed unpaired t-test with Welch's correction. When three or more groups were compared, one-way ANOVA with Bonferroni post hoc test or two-way ANOVA was used. A P value less than 0.05 was considered significant. The analyses were done in GraphPad Prism v.5.

Acknowledgements
This work was in part supported by grants from the NIH (R21HD091512 and R01NS102382 to P.J.) R.P.H. was supported by R01ES026057, R01AA023797, and U10AA008401. We would like to thank Dr. Brian Daniels from Rutgers University for critical reading of the manuscript.

Author Contributions
P.J. and R.X. designed experiments and interpreted data; R.X. carried out most of experiments with technical assistance from A.B., A.P., and K.K.; R.P.H. performed the gene expression analysis, interpreted the data, and provided critical suggestions to the overall research direction; P.J. directed the project and wrote the manuscript together with R.X. and input from all co-authors.

Competing Financial Interests
The authors declare no competing financial interests.

Figure legends:

Figure 1. Generation of hPSC microglial chimeric mouse brains.
(A) A schematic procedure for generating primitive macrophage precursor (PMP) from hiPSCs or hESCs-derived yolk sac embryoid bodies (YS-EB). Insets: representative bright-field images at different stages. Scale bars represent 100 μm, 200 μm, and 20 μm as indicated in the images
(B) Representative images and quantification of $CD235^+$, $CD43^+$, $CD235^+/CD43^+$, and $Ki67^+$ cells in PMP. Quantification of pooled data from one hiPSC line and one hESC line. The experiments are repeated for four times (n = 4) and for each experiment, the two stem cell lines are used. Data are presented as mean ± s.e.m. Scale bars: 20 μm in the original and enlarged images.
(C) A schematic diagram showing that hPSC-derived PMP are engrafted into the brains of P0 *rag*$2^{-/-}$ hCSF1 mice.
(D) Representative images from sagittal brain sections showing the wide distribution of xenografted hPSC-derived microglia at six months post-transplantation. Anti-human-specific TMEM119 (hTMEM119) selectively labels xenografted hPSC-derived microglia. Scale bar: 1 mm.
(E-H) Representative images from sagittal brain sections showing the distribution of $hTMEM119^+$ xenografted hPSC-derived microglia at 3 weeks and 6 months post-transplantation in different brain regions. OB, olfactory bulb; RMS, rostral migratory stream; CC, corpus callosum; Hippo, Hippocampus. Scale bars: 1 mm or 50 μm in the original or enlarged images, respectively.
(I) Representative images of $hTMEM119^+$ cells among the total donor-derived hN^+ cells in grey matter at 8 weeks post-transplantation. Scale bars, 50 μm or 20 μm in the original or enlarged images, respectively.
(J) Representative images of PU.1- and human-specific CD45 (hCD45)-expressing cells in the donor-derived $hTMEM119^+$ cells in different brain regions at 8 weeks post-transplantation. Scale bars, 50 μm or 20 μm in the original or enlarged images, respectively.
(L) Quantification of the percentage of hN^+ cells in total $DAPI^+$ cells in the forebrain at 6 months post-transplantation (n = 10 mice). The data are pooled from the mice received transplantation of microglia derived from both hESCs and hiPSCs. Data are presented as mean ± s.e.m.
(M) Quantification of the percentage of $hTMEM119^+$ cells in total hN^+ cells (n = 7 mice). Data are presented as mean ± s.e.m.
(N) Quantification of $Ki67^+$ cells among the total donor-derived hN^+ cells at 3 weeks or 6 months post-transplantation (n = 8 mice for each time point). The data are pooled from the mice received transplantation of microglia derived from both hESCs and hiPSCs. Student's *t* test. $^{**}P < 0.01$. Data are presented as mean ± s.e.m.

Figure 2. Human PSC-derived microglia undergo morphological maturation and are functional in the mouse brain.
(A) Representative images of $hTMEM119^+$ hPSC-derived microglia and $mTMEM119^+$ mouse microglia in the cerebral cortex, corpus callosum (CC) and hippocampus (HIP) in 6 months old mice. Scale bars represent 200 μm and 50 μm in the original and enlarged images, respectively.
(B) Representative images of $hTMEM119^+$ hPSC-derived microglia and $mTMEM119^+$ mouse microglia in the cerebral cortex at 3 weeks, 8 weeks, and 6 months old mice. Scale bars represent 50 μm and 20 μm in the original and enlarged images, respectively.
(C and D) Quantification of endpoint numbers, total process length of mouse and hPSC-derived microglia based on mTMEM119 or hTMEM119 staining respectively from grey matter at 3 weeks, 8 weeks, and 6 months old mice (n = 7 mice for each time point). The data are pooled from the mice received transplantation of microglia derived from both hESCs and hiPSCs. One-way ANOVA test, $^{*}P < 0.05$, $^{***}P < 0.001$, NS, no significance. Data are presented as mean ± s.e.m.
(E) Quantification of the percentage of $CD68^+$ area in $hTMEM119^+$ area from cerebral cortex at 3 weeks, 8 weeks and 6 months old chimeric mice (n = 7 mice for each time point). One-way ANOVA test, $^{**}P < 0.01$, $^{***}P < 0.001$. Data are presented as mean ± s.e.m.

(F) Quantification of PSD95$^+$ fraction engulfed per microglia from cerebral cortex at 3 weeks, 8 weeks and 6 months old chimeric mice (n = 7 mice for each time point). One-way ANOVA test, *P < 0.05. Data are presented as mean ± s.e.m.
(G) Representative images of CD68- and hTMEM119-exprssing cells (the left three columns) in the cerebral cortex and 3D reconstruction images showing hCD45$^+$ donor-derived microglia with post-synaptic marker, PSD95 (the rightmost column) from 3 weeks, 8 weeks and 6 months old mice. Scale bars, 10 μm or 2 μm in the original or enlarged images, respectively.
(H) Representative images showing the interactions between blood vessels and hPSC-derived microglia in grey matter and white matter at 8 weeks post-transplantation. Laminin labels blood vessels and hCD45 marks hPSC-derived microglia. Scale bars, 50 and 20 μm in the original or enlarged images, respectively.

Figure 3. Single-cell RNA-sequencing of hiPSC microglial chimeric mouse brain identifies gene expression signatures of adult human microglia
(A) A schematic diagram showing the experimental design. Microglia were isolated from the highlighted brain regions at 6 months post-transplantation and handled at 4°C to reduce ex vivo activation. The single-cell suspension was loaded into a 10X Genomics Chromium system for single-cell RNA-sequencing.
(B) tSNE plot of 11 cell types as identified by characteristic cell-specific gene expression, following translation of human gene symbols to mouse symbols as described in Methods. Arrow indicates the human xenograft microglia (Xeno MG).
(C) Dot plot showing two representative cell-specific genes for each cell cluster. As indicated by the legend, the diameter of the dot indicates the percent of cells within a cluster expressing the gene (pct.exp). The color saturation indicates the average expression over the cluster (avg.exp; log normalized counts). The cluster numbers, colors of clusters in panel B, and selected cell identities are shown at left.
(D) tSNE plots with dots (representing individual barcodes/cells) colored by expression of canonical microglial genes, based on expression level determined in Seurat (log normalized counts).
(E) A heatmap showing average expression of the top 30 human microglial signature genes [8] in each of the 11 cell clusters. Expression of each gene was expressed as a Z-score (normalized to average expression) to compare relative expression differences by cell type.
(F) Principal component analysis (PCA) of Xeno MGs (pink), and individual cell RNA-seq expression data from publicly-available datasets, including human adult microglia (Adult MG) from Ormel et al., 2018 [67] (orange) and Galatro et al., 2017 [12] (blue), human fetal microglia (Fetal MG; light green), iPSC-derived 2D microglia (iPS MG, green), blood macrophage (ochre), and liver macrophage (cyan) from Douvaras et al., 2017 [17], and hiPSC-derived 3D organoid microglia from Ormel et al., 2018 [67] (oMG, violet), using the 547 genes identified as age-related genes in microglia by Galatro et. al., 2017 [12]. PCA analysis demonstrates that Xeno MG have the most similarity to Adult MG, compared with other clusters, and is clearly separated from Blood/Liver macrophage.
(G) t-SNE plots of selected human cells showing the expression of *CD74, SPP1, C3, BAZ2B, CCL4, EGR2, EGR3,* and *CD83* gene transcripts. *CD74*, *SPP1*, *C3* and *BAZ2B* appear to be uniformly expressed in all cells, but *CCL4, EGR2, EGR3,* and *CD83* are enriched in distinct subsets of in Xeno MG.

Figure 4. Transcriptomic profiling analysis reveals differences between adult human and mouse microglia
(A) tSNE plot highlighting only the clusters of human Xeno MG and mouse host microglia.
(B) Scatter plot showing mRNA expression levels of human and mouse genes with unique orthologs from Xeno MG and mouse microglia clusters, highlighting the differentially expressed genes (DEGs; at least two-fold different) in human Xeno MG (red) or mouse microglia (green) from 6 month old chimeric

mouse brain. Significantly different DEGs (less than 5% false discovery rate [FDR] and at least two-fold different) are listed in Supplementary Table 2.
(C) Violin plots summarizing expression differences in individual cells within the human Xeno MG and mouse microglia clusters. Dots indicate expression levels (as log normalized counts) of individual cells and the violin shape summarizes the distribution of expression in the population.
(D) A heatmap showing the DEGs in individual samples (n = 4) of human and mouse microglia from 6 month old chimeric mouse brains. Expression levels (log normalized counts) were normalized to mean expression of all samples, producing a Z-score, with color assignments indicated by the legend.
(E) Enriched gene ontology (GO) biological process terms for the upregulated DEGs in human Xeno MG, plotted as the $-\log_{10}$ (p-value) of enrichment [94].
(F and G) Bar plots showing the average expression (mean ± SEM, n = 4 samples) of Alzheimer's disease (AD; F) or Parkinson's disease (PD; G)-associated genes in Xeno MG and mouse microglia. These genes were reported to be differentially expressed between human and mouse microglia as in Gosselin et al., 2017 [8].
(H) Venn diagrams showing that majority of the genes that were reported to be differentially expressed between human and mouse microglia are recapitulated in our chimeric mouse model (10 out of 14 for AD; 18 out of 20 for PD).

Supplementary figure Legends:

Supplementary Figure 1. Identification of hPSC-derived microglia in the mouse brain.
(A) Representative images showing the morphology of hTMEM119$^+$ hPSC-derived microglia in the cerebral cortex, hippocampus (HIP), olfactory bulb (OB), cerebellum (CB) and white matter (WM) at 6 months post-transplantation. CC: corpus callosum. Scale bars: 50 μm or 20 μm in the original or enlarged images, respectively.
(B) Representative images of Ki67- and hN-expressing cells in the OB, lateral walls of lateral ventricle (LV), and WM at 6 months post-transplantation. Scale bars, 50 μm or 20 μm in the original or enlarged images, respectively.

Supplementary Figure 2. Characterization of the function of hPSC-derived microglia in the mouse brain.
(A) Representative images of Iba1$^+$/hN$^+$ hPSC-derived microglia in the grey matter (GM), white matter (WM) and olfactory bulb (OB) at 3 weeks and 8 weeks post-transplantation. CC: corpus callosum. Scale bars, 20 μm in both the original and enlarged images.
(B) Representative 3D reconstruction images showing that hCD45$^+$ hPSC-derived microglia phagocytize Olig2$^+$ oligodendroglial cells in the CC at 3 weeks post-transplantation. Scale bars, 5 μm.
(C) Representative images showing the interactions between laminin$^+$ blood vessels and hPSC-derived microglia in the OB at 8 weeks post-transplantation. Scale bars, 50 μm.

Supplementary Figure 3. Single-cell RNA-sequencing of hiPSC microglial chimeric mouse brains.
(A) A table summarizing the observed numbers of single-cell RNA-sequencing reads and those matching human (hg19) or mouse (mm10) genome with high confidence.
(B) tSNE plots showing that the 11 cell type clusters are reproducibly identified in each of the four sampled 6-month-old chimeric mouse brains.
(C) tSNE plot showing the expression of representative genes in each of the 11 clusters. Blue color saturation indicates relative log normalized counts in each cell (dot, as identified by unique barcode).
(D) A pie chart summarizing the numbers of cells (barcodes) identified within each clustered cell type.
(E) Scatter plot array showing the pairwise correlation of average expression for each cell type. Notably, the Xeno MG and mouse microglia clusters had the highest correlation coefficient value, 0.765.

Supplementary Figure 4. Transcriptomic profile of Xeno MG developed in the mouse brain.
(A) Scatter plot showing correlation of human Xeno microglia with human adult microglia dataset reported in Galatro et. al., 2017. Expression levels are normalized reads per million (RPM). The 10X Genomics data from the Human Xeno MG matched only the relatively higher levels of expression ($\log_2$ RPM > 2) of the deeper (more RNAseq reads per sample) dataset from Galatro. However, transcripts above this threshold exhibited a strong correlation ($r^2 = 0.3851$, $p < 2.2 \times 10^{-16}$).
(B) t-SNE plots for mRNA expression of acute pro-inflammatory cytokines, *IL-1β, IL-1α,* and *TNF-α,* and chronic pro-inflammatory cytokine, *IL-6* and anti-inflammatory cytokine, *IL-10*.
(C) t-SNE plots for *CST3, P2RY13, EGR1,* and *MCL1* mRNA expression (log normalized counts) within the selected human Xeno MG cluster.
(D) Bar plots showing the expression (mean ± SEM, n = 4) of multiple sclerosis (MS) or schizophrenia (SCZ)-associated genes in Xeno MG and mouse microglia. All these genes were reported to be differentially expressed between human and mouse microglia in Gosselin et al., 2017 [8].
(E) Venn diagram showing that the majority of genes that were reported to be differentially expressed between human and mouse microglia are recapitulated in our chimeric mouse model (29 of 32 for MS; 34 of 42 for SCZ).

References:

1. Li, Q. & Barres, B.A. Microglia and macrophages in brain homeostasis and disease. *Nat Rev Immunol* **18**, 225-242 (2018).
2. Casano, A.M. & Peri, F. Microglia: multitasking specialists of the brain. *Dev Cell* **32**, 469-477 (2015).
3. Keren-Shaul, H. et al. A Unique Microglia Type Associated with Restricting Development of Alzheimer's Disease. *Cell* **169**, 1276-1290 e1217 (2017).
4. Hong, S. et al. Complement and microglia mediate early synapse loss in Alzheimer mouse models. *Science* **352**, 712-716 (2016).
5. Yeh, F.L., Wang, Y., Tom, I., Gonzalez, L.C. & Sheng, M. TREM2 Binds to Apolipoproteins, Including APOE and CLU/APOJ, and Thereby Facilitates Uptake of Amyloid-Beta by Microglia. *Neuron* **91**, 328-340 (2016).
6. Venegas, C. et al. Microglia-derived ASC specks cross-seed amyloid-beta in Alzheimer's disease. *Nature* **552**, 355-361 (2017).
7. Fuhrmann, M. et al. Microglial Cx3cr1 knockout prevents neuron loss in a mouse model of Alzheimer's disease. *Nat Neurosci* **13**, 411-413 (2010).
8. Gosselin, D. et al. An environment-dependent transcriptional network specifies human microglia identity. *Science* **356** (2017).
9. Hansen, D.V., Hanson, J.E. & Sheng, M. Microglia in Alzheimer's disease. *The Journal of cell biology* **217**, 459-472 (2018).
10. Holtman, I.R., Skola, D. & Glass, C.K. Transcriptional control of microglia phenotypes in health and disease. *J Clin Invest* **127**, 3220-3229 (2017).
11. Smith, A.M. & Dragunow, M. The human side of microglia. *Trends Neurosci* **37**, 125-135 (2014).
12. Galatro, T.F. et al. Transcriptomic analysis of purified human cortical microglia reveals age-associated changes. *Nat Neurosci* **20**, 1162-1171 (2017).
13. Friedman, B.A. et al. Diverse Brain Myeloid Expression Profiles Reveal Distinct Microglial Activation States and Aspects of Alzheimer's Disease Not Evident in Mouse Models. *Cell Rep* **22**, 832-847 (2018).
14. Muffat, J. et al. Efficient derivation of microglia-like cells from human pluripotent stem cells. *Nat Med* **22**, 1358-1367 (2016).
15. Pandya, H. et al. Differentiation of human and murine induced pluripotent stem cells to microglia-like cells. *Nat Neurosci* **20**, 753-759 (2017).
16. Abud, E.M. et al. iPSC-Derived Human Microglia-like Cells to Study Neurological Diseases. *Neuron* **94**, 278-293 e279 (2017).
17. Douvaras, P. et al. Directed Differentiation of Human Pluripotent Stem Cells to Microglia. *Stem Cell Reports* **8**, 1516-1524 (2017).
18. Haenseler, W. et al. A Highly Efficient Human Pluripotent Stem Cell Microglia Model Displays a Neuronal-Co-culture-Specific Expression Profile and Inflammatory Response. *Stem Cell Reports* **8**, 1727-1742 (2017).
19. Brownjohn, P.W. et al. Functional Studies of Missense TREM2 Mutations in Human Stem Cell-Derived Microglia. *Stem Cell Reports* **10**, 1294-1307 (2018).
20. Olah, M. et al. A transcriptomic atlas of aged human microglia. *Nature communications* **9**, 539 (2018).

21. Chen, C., Kim, W.Y. & Jiang, P. Humanized neuronal chimeric mouse brain generated by neonatally engrafted human iPSC-derived primitive neural progenitor cells. *JCI Insight* **1**, e88632 (2016).
22. Xu, R. et al. Reversing Abnormal Neural Development by Inhibiting OLIG2 in Down Syndrome Human iPSC Brain Organoids and Neuronal Mouse Chimeras. *BioRxiv* (2018).
23. Windrem, M.S. et al. Human iPSC Glial Mouse Chimeras Reveal Glial Contributions to Schizophrenia. *Cell Stem Cell* **21**, 195-208 e196 (2017).
24. Han, X. et al. Forebrain engraftment by human glial progenitor cells enhances synaptic plasticity and learning in adult mice. *Cell Stem Cell* **12**, 342-353 (2013).
25. Chen, H. et al. Human-derived neural progenitors functionally replace astrocytes in adult mice. *J Clin Invest* **125**, 1033-1042 (2015).
26. Claes, C., Van den Daele, J. & Verfaillie, C.M. Generating tissue-resident macrophages from pluripotent stem cells: Lessons learned from microglia. *Cell Immunol* **330**, 60-67 (2018).
27. Sturgeon, C.M., Ditadi, A., Awong, G., Kennedy, M. & Keller, G. Wnt signaling controls the specification of definitive and primitive hematopoiesis from human pluripotent stem cells. *Nat Biotechnol* **32**, 554-561 (2014).
28. Bennett, M.L. et al. New tools for studying microglia in the mouse and human CNS. *Proc Natl Acad Sci U S A* **113**, E1738-1746 (2016).
29. Kettenmann, H., Hanisch, U.K., Noda, M. & Verkhratsky, A. Physiology of microglia. *Physiol Rev* **91**, 461-553 (2011).
30. Forrester, J.V., McMenamin, P.G. & Dando, S.J. CNS infection and immune privilege. *Nat Rev Neurosci* **19**, 655-671 (2018).
31. McKercher, S.R. et al. Targeted disruption of the PU.1 gene results in multiple hematopoietic abnormalities. *EMBO J* **15**, 5647-5658 (1996).
32. Kim, E.M., Manzar, G. & Zavazava, N. Human iPS cell-derived hematopoietic progenitor cells induce T-cell anergy in in vitro-generated alloreactive CD8(+) T cells. *Blood* **121**, 5167-5175 (2013).
33. Smith, A.M. et al. The transcription factor PU.1 is critical for viability and function of human brain microglia. *Glia* **61**, 929-942 (2013).
34. Feng, R. et al. PU.1 and C/EBPalpha/beta convert fibroblasts into macrophage-like cells. *Proc Natl Acad Sci U S A* **105**, 6057-6062 (2008).
35. Ford, A.L., Goodsall, A.L., Hickey, W.F. & Sedgwick, J.D. Normal adult ramified microglia separated from other central nervous system macrophages by flow cytometric sorting. Phenotypic differences defined and direct ex vivo antigen presentation to myelin basic protein-reactive CD4+ T cells compared. *J Immunol* **154**, 4309-4321 (1995).
36. Pirzgalska, R.M. et al. Sympathetic neuron-associated macrophages contribute to obesity by importing and metabolizing norepinephrine. *Nat Med* **23**, 1309-1318 (2017).
37. Lawson, L.J., Perry, V.H., Dri, P. & Gordon, S. Heterogeneity in the distribution and morphology of microglia in the normal adult mouse brain. *Neuroscience* **39**, 151-170 (1990).
38. Marsh, S.E. et al. The adaptive immune system restrains Alzheimer's disease pathogenesis by modulating microglial function. *Proc Natl Acad Sci U S A* **113**, E1316-1325 (2016).
39. Hanisch, U.K. & Kettenmann, H. Microglia: active sensor and versatile effector cells in the normal and pathologic brain. *Nat Neurosci* **10**, 1387-1394 (2007).
40. Colonna, M. & Butovsky, O. Microglia Function in the Central Nervous System During Health and Neurodegeneration. *Annu Rev Immunol* **35**, 441-468 (2017).

41. Weinhard, L. et al. Microglia remodel synapses by presynaptic trogocytosis and spine head filopodia induction. *Nat Commun* **9**, 1228 (2018).
42. Paolicelli, R.C. et al. Synaptic pruning by microglia is necessary for normal brain development. *Science* **333**, 1456-1458 (2011).
43. Schafer, D.P. & Stevens, B. Microglia Function in Central Nervous System Development and Plasticity. *Cold Spring Harb Perspect Biol* **7**, a020545 (2015).
44. Li, Q.Y. et al. Developmental Heterogeneity of Microglia and Brain Myeloid Cells Revealed by Deep Single-Cell RNA Sequencing. *Neuron* **101**, 207-+ (2019).
45. Eriksdotter-Nilsson, M., Bjorklund, H. & Olson, L. Laminin immunohistochemistry: a simple method to visualize and quantitate vascular structures in the mammalian brain. *J Neurosci Methods* **17**, 275-286 (1986).
46. Zhang, Y. et al. Purification and Characterization of Progenitor and Mature Human Astrocytes Reveals Transcriptional and Functional Differences with Mouse. *Neuron* **89**, 37-53 (2016).
47. Dulken, B.W., Leeman, D.S., Boutet, S.C., Hebestreit, K. & Brunet, A. Single-Cell Transcriptomic Analysis Defines Heterogeneity and Transcriptional Dynamics in the Adult Neural Stem Cell Lineage. *Cell Rep* **18**, 777-790 (2017).
48. Tkachev, D. et al. Oligodendrocyte dysfunction in schizophrenia and bipolar disorder. *Lancet* **362**, 798-805 (2003).
49. Lee, J., Gravel, M., Zhang, R., Thibault, P. & Braun, P.E. Process outgrowth in oligodendrocytes is mediated by CNP, a novel microtubule assembly myelin protein. *The Journal of cell biology* **170**, 661-673 (2005).
50. Wang, S. et al. Human iPSC-derived oligodendrocyte progenitor cells can myelinate and rescue a mouse model of congenital hypomyelination. *Cell Stem Cell* **12**, 252-264 (2013).
51. Liu, M.L. et al. Small molecules enable neurogenin 2 to efficiently convert human fibroblasts into cholinergic neurons. *Nat Commun* **4**, 2183 (2013).
52. Sherriff, F.E., Bridges, L.R., Gentleman, S.M., Sivaloganathan, S. & Wilson, S. Markers of axonal injury in post mortem human brain. *Acta neuropathologica* **88**, 433-439 (1994).
53. Bergsland, M., Werme, M., Malewicz, M., Perlmann, T. & Muhr, J. The establishment of neuronal properties is controlled by Sox4 and Sox11. *Genes Dev* **20**, 3475-3486 (2006).
54. Fuzik, J. et al. Integration of electrophysiological recordings with single-cell RNA-seq data identifies neuronal subtypes. *Nat Biotechnol* **34**, 175-183 (2016).
55. Sweeney, M.D., Kisler, K., Montagne, A., Toga, A.W. & Zlokovic, B.V. The role of brain vasculature in neurodegenerative disorders. *Nat Neurosci* **21**, 1318-1331 (2018).
56. Bostrom, K.I. Cell differentiation in vascular calcification. *Z Kardiol* **89 Suppl 2**, 69-74 (2000).
57. Marques, F. et al. Lipocalin 2 is a choroid plexus acute-phase protein. *J Cereb Blood Flow Metab* **28**, 450-455 (2008).
58. Marques, F. et al. Transcriptome signature of the adult mouse choroid plexus. *Fluids Barriers CNS* **8**, 10 (2011).
59. Arneson, D. et al. Single cell molecular alterations reveal target cells and pathways of concussive brain injury. *Nat Commun* **9**, 3894 (2018).
60. Daneman, R. et al. The mouse blood-brain barrier transcriptome: a new resource for understanding the development and function of brain endothelial cells. *PLoS One* **5**, e13741 (2010).

61. Tremblay, R., Lee, S. & Rudy, B. GABAergic Interneurons in the Neocortex: From Cellular Properties to Circuits. *Neuron* **91**, 260-292 (2016).
62. Hu, J.S. et al. Coup-TF1 and Coup-TF2 control subtype and laminar identity of MGE-derived neocortical interneurons. *Development* **144**, 2837-2851 (2017).
63. Pan, J.Z. et al. Cytokine activity contributes to induction of inflammatory cytokine mRNAs in spinal cord following contusion. *J Neurosci Res* **68**, 315 (2002).
64. Feghali, C.A. & Wright, T.M. Cytokines in acute and chronic inflammation. *Front Biosci* **2**, d12-26 (1997).
65. Turner, M.D., Nedjai, B., Hurst, T. & Pennington, D.J. Cytokines and chemokines: At the crossroads of cell signalling and inflammatory disease. *Biochim Biophys Acta* **1843**, 2563-2582 (2014).
66. Yamamizu, K. et al. In Vitro Modeling of Blood-Brain Barrier with Human iPSC-Derived Endothelial Cells, Pericytes, Neurons, and Astrocytes via Notch Signaling. *Stem Cell Reports* **8**, 634-647 (2017).
67. Ormel, P.R. et al. Microglia innately develop within cerebral organoids. *Nature communications* **9**, 4167 (2018).
68. Masuda, T. et al. Spatial and temporal heterogeneity of mouse and human microglia at single-cell resolution. *Nature* **566**, 388-392 (2019).
69. Wolf, S.A., Boddeke, H.W. & Kettenmann, H. Microglia in Physiology and Disease. *Annu Rev Physiol* **79**, 619-643 (2017).
70. Butovsky, O. & Weiner, H.L. Microglial signatures and their role in health and disease. *Nat Rev Neurosci* **19**, 622-635 (2018).
71. Ito, R., Takahashi, T. & Ito, M. Humanized mouse models: Application to human diseases. *J Cell Physiol* **233**, 3723-3728 (2018).
72. Askew, K. et al. Coupled Proliferation and Apoptosis Maintain the Rapid Turnover of Microglia in the Adult Brain. *Cell Rep* **18**, 391-405 (2017).
73. Tay, T.L. et al. A new fate mapping system reveals context-dependent random or clonal expansion of microglia. *Nat Neurosci* **20**, 793-803 (2017).
74. Reu, P. et al. The Lifespan and Turnover of Microglia in the Human Brain. *Cell Rep* **20**, 779-784 (2017).
75. Windrem, M.S. et al. A competitive advantage by neonatally engrafted human glial progenitors yields mice whose brains are chimeric for human glia. *J Neurosci* **34**, 16153-16161 (2014).
76. McQuade, A. et al. Development and validation of a simplified method to generate human microglia from pluripotent stem cells. *Mol Neurodegener* **13**, 67 (2018).
77. Stevens, B. et al. The classical complement cascade mediates CNS synapse elimination. *Cell* **131**, 1164-1178 (2007).
78. Cunningham, C.L., Martinez-Cerdeno, V. & Noctor, S.C. Microglia regulate the number of neural precursor cells in the developing cerebral cortex. *J Neurosci* **33**, 4216-4233 (2013).
79. Thion, M.S., Ginhoux, F. & Garel, S. Microglia and early brain development: An intimate journey. *Science* **362**, 185-189 (2018).
80. Elmore, M.R. et al. Colony-stimulating factor 1 receptor signaling is necessary for microglia viability, unmasking a microglia progenitor cell in the adult brain. *Neuron* **82**, 380-397 (2014).
81. Gowing, G., Vallieres, L. & Julien, J.P. Mouse model for ablation of proliferating microglia in acute CNS injuries. *Glia* **53**, 331-337 (2006).

82. Lan, P., Tonomura, N., Shimizu, A., Wang, S. & Yang, Y.G. Reconstitution of a functional human immune system in immunodeficient mice through combined human fetal thymus/liver and CD34+ cell transplantation. *Blood* **108**, 487-492 (2006).
83. Slukvin, II Hematopoietic specification from human pluripotent stem cells: current advances and challenges toward de novo generation of hematopoietic stem cells. *Blood* **122**, 4035-4046 (2013).
84. Chen, C. et al. Role of astroglia in Down's syndrome revealed by patient-derived human-induced pluripotent stem cells. *Nature communications* **5**, 4430 (2014).
85. Muller, F.J. et al. A bioinformatic assay for pluripotency in human cells. *Nat Methods* **8**, 315-317 (2011).
86. Marques, S. et al. Oligodendrocyte heterogeneity in the mouse juvenile and adult central nervous system. *Science* **352**, 1326-1329 (2016).
87. Butler, A. & Satija, R. Integrated analysis of single cell transcriptomic data across conditions, technologies, and species. *bioRxiv*, 164889 (2017).
88. Macosko, E.Z. et al. Highly Parallel Genome-wide Expression Profiling of Individual Cells Using Nanoliter Droplets. *Cell* **161**, 1202-1214 (2015).
89. Satija, R., Farrell, J.A., Gennert, D., Schier, A.F. & Regev, A. Spatial reconstruction of single-cell gene expression data. *Nat Biotechnol* **33**, 495-502 (2015).
90. Gentleman, R.C. et al. Bioconductor: open software development for computational biology and bioinformatics. *Genome Biol* **5**, R80 (2004).
91. Butler, A., Hoffman, P., Smibert, P., Papalexi, E. & Satija, R. Integrating single-cell transcriptomic data across different conditions, technologies, and species. *Nat Biotechnol* **36**, 411-420 (2018).
92. Kim, D., Langmead, B. & Salzberg, S.L. HISAT: a fast spliced aligner with low memory requirements. *Nature methods* **12**, 357-360 (2015).
93. Love, M.I., Huber, W. & Anders, S. Moderated estimation of fold change and dispersion for RNA-seq data with DESeq2. *Genome Biol* **15**, 550 (2014).
94. Reimand, J. et al. g:Profiler-a web server for functional interpretation of gene lists (2016 update). *Nucleic Acids Res* **44**, W83-89 (2016).
95. Pasca, A.M. et al. Functional cortical neurons and astrocytes from human pluripotent stem cells in 3D culture. *Nature methods* **12**, 671-678 (2015).
96. Liu, Y., Jiang, P. & Deng, W. OLIG gene targeting in human pluripotent stem cells for motor neuron and oligodendrocyte differentiation. *Nat Protoc* **6**, 640-655 (2011).

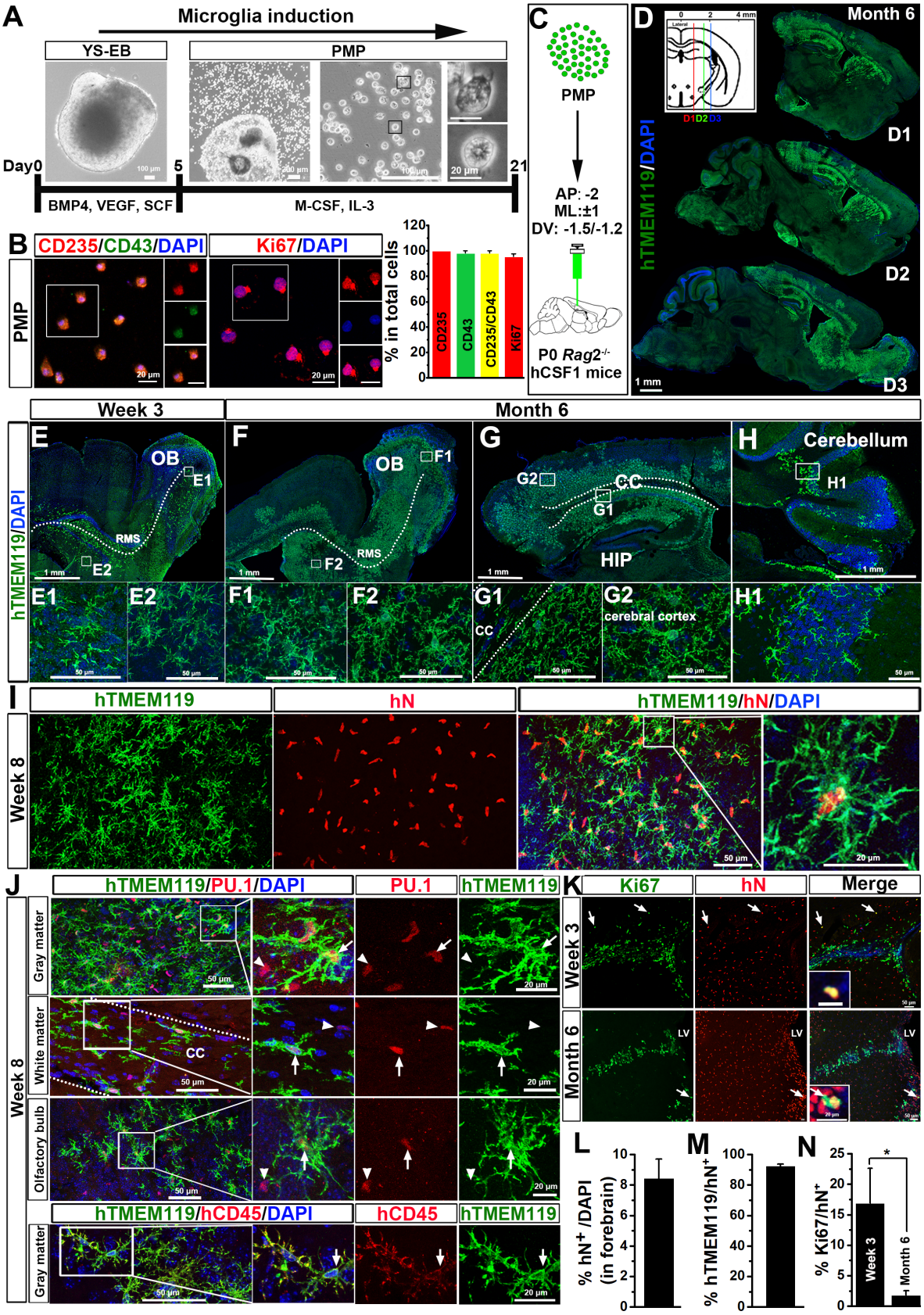
A
Microglia induction
YS-EB
PMP
Day0
5
21
BMP4, VEGF, SCF
M-CSF, IL-3
B
CD235/CD43/DAPI
Ki67/DAPI
PMP
% in total cells
CD235
CD43
CD235/CD43
Ki67
C
PMP
AP: -2
ML:±1
DV: -1.5/-1.2
P0 Rag2-/-
hCSF1 mice
D
Month 6
hTMEM119/DAPI
D1
D2
D3
1 mm
Week 3
Month 6
E
OB
E1
RMS
E2
F
OB
F1
RMS
F2
G
G2
CC
G1
HIP
H
Cerebellum
H1
E1
E2
F1
F2
G1
CC
G2
cerebral cortex
H1
I
Week 8
hTMEM119
hN
hTMEM119/hN/DAPI
J
hTMEM119/PU.1/DAPI
PU.1
hTMEM119
Gray matter
White matter
Olfactory bulb
CC
hTMEM119/hCD45/DAPI
hCD45
hTMEM119
K
Ki67
hN
Merge
Week 3
Month 6
LV
L
% hN+ /DAPI (in forebrain)
M
% hTMEM119/hN+
N
% Ki67/hN+
Week 3
Month 6
*

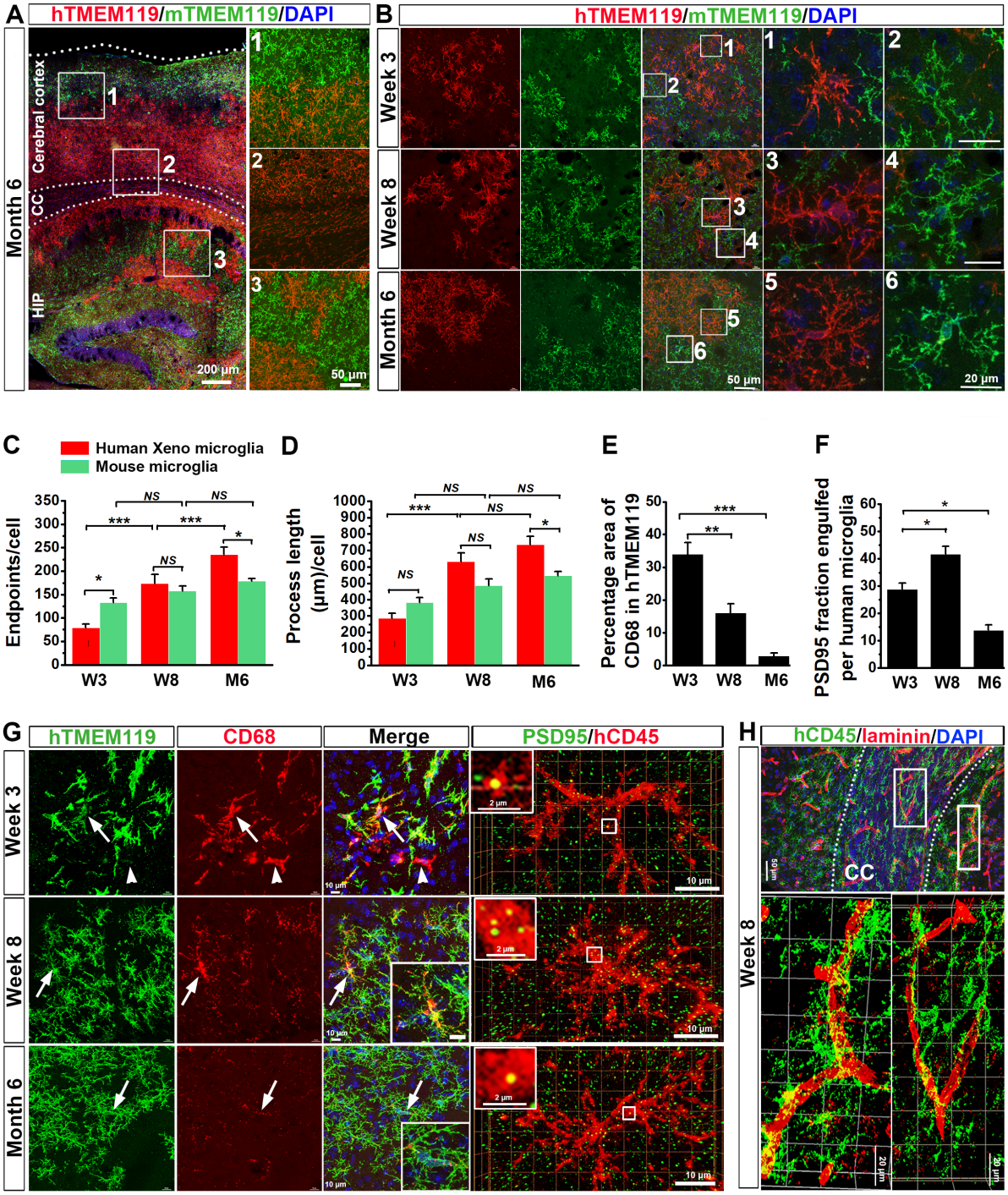
A
hTMEM119/mTMEM119/DAPI
Month 6
Cerebral cortex
CC
HIP
200 µm
50 µm
B
hTMEM119/mTMEM119/DAPI
Week 3
Week 8
Month 6
50 µm
20 µm
C
Human Xeno microglia
Mouse microglia
Endpoints/cell
W3
W8
M6
D
Process length (µm)/cell
E
Percentage area of CD68 in hTMEM119
F
PSD95 fraction engulfed per human microglia
G
hTMEM119
CD68
Merge
PSD95/hCD45
Week 3
Week 8
Month 6
10 µm
2 µm
H
hCD45/laminin/DAPI
Week 8
CC
50 µm
20 µm

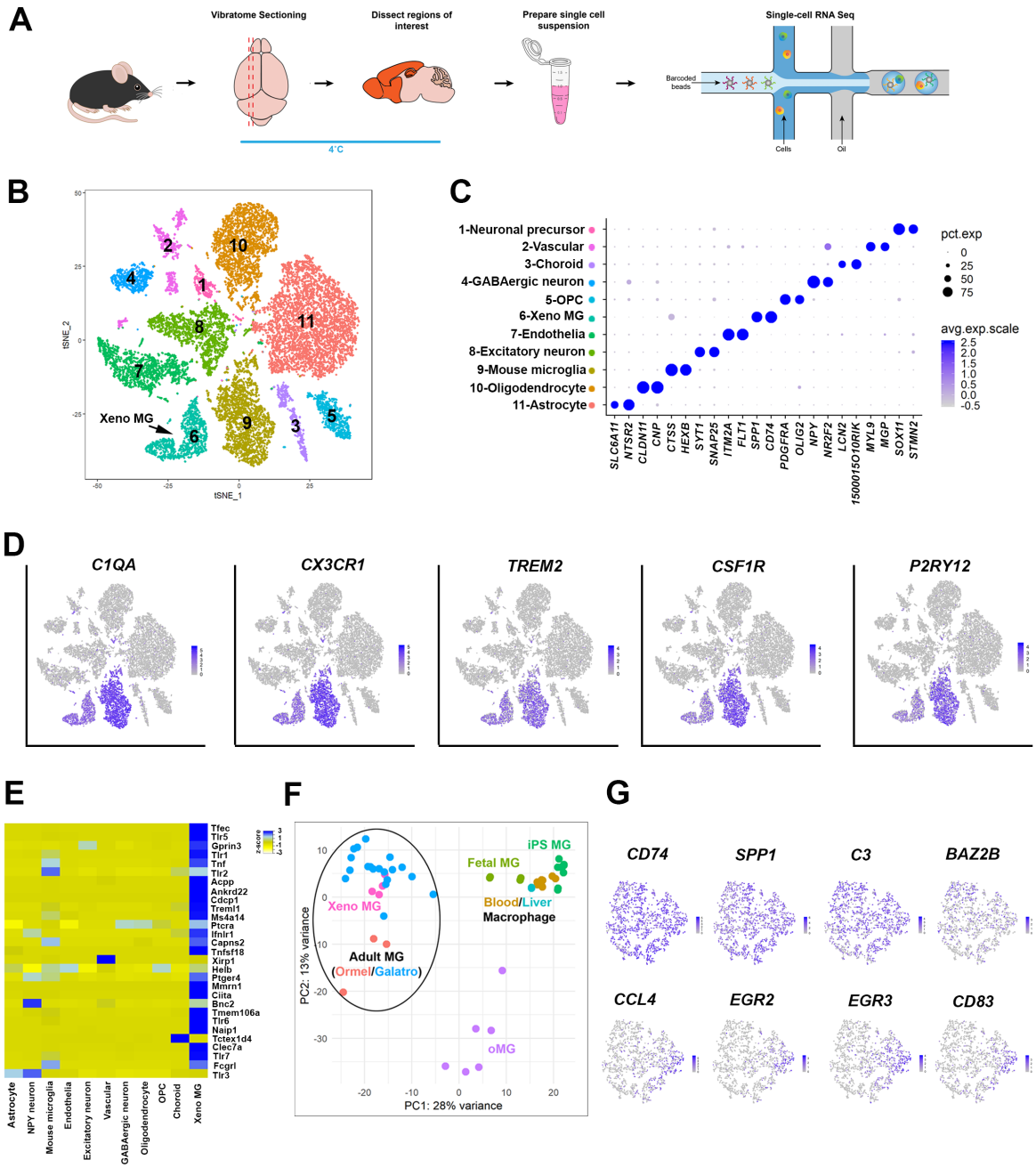
A
Vibratome Sectioning
Dissect regions of interest
Prepare single cell suspension
Single-cell RNA Seq
Barcoded beads
Cells
Oil
4°C
B
tSNE_1
tSNE_2
Xeno MG
C
1-Neuronal precursor
2-Vascular
3-Choroid
4-GABAergic neuron
5-OPC
6-Xeno MG
7-Endothelia
8-Excitatory neuron
9-Mouse microglia
10-Oligodendrocyte
11-Astrocyte
SLC6A11
NTSR2
CLDN11
CNP
CTSS
HEXB
SYT1
SNAP25
ITM2A
FLT1
SPP1
CD74
PDGFRA
OLIG2
NPY
NR2F2
LCN2
15000150 10RIK
MYL9
MGP
SOX11
STMN2
pct.exp
avg.exp.scale
D
C1QA
CX3CR1
TREM2
CSF1R
P2RY12
E
Astrocyte
NPY neuron
Mouse microglia
Endothelia
Excitatory neuron
Vascular
GABAergic neuron
Oligodendrocyte
OPC
Choroid
Xeno MG
F
PC1: 28% variance
PC2: 13% variance
iPS MG
Fetal MG
Xeno MG
Blood/Liver Macrophage
Adult MG (Ormel/Galatro)
oMG
G
CD74
SPP1
C3
BAZ2B
CCL4
EGR2
EGR3
CD83

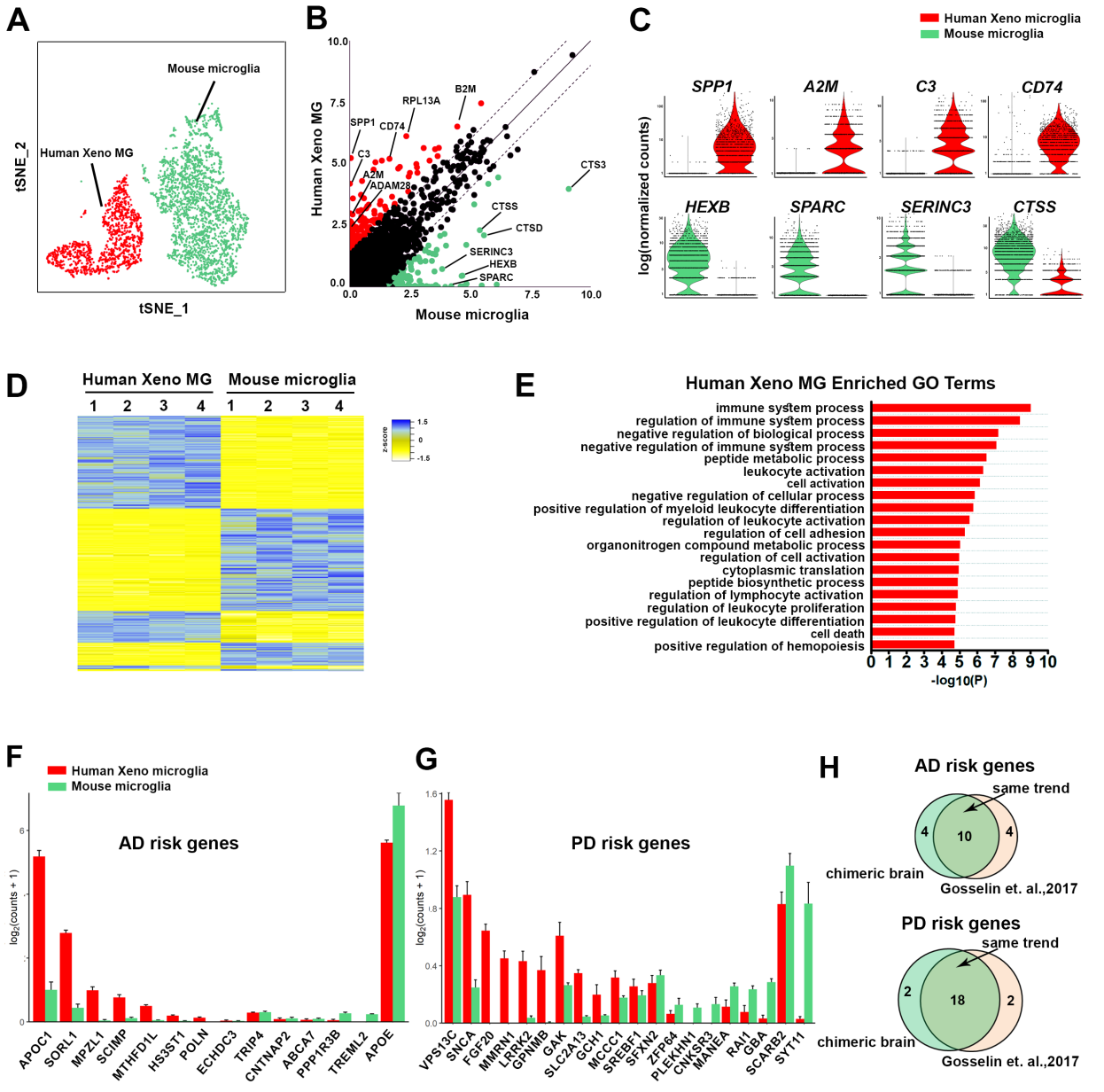
A
Mouse microglia
Human Xeno MG
tSNE_2
tSNE_1
B
Human Xeno MG
Mouse microglia
SPP1
C3
A2M
ADAM28
CD74
RPL13A
B2M
CTS3
CTSS
CTSD
SERINC3
HEXB
SPARC
C
Human Xeno microglia
Mouse microglia
log(normalized counts)
SPP1
A2M
C3
CD74
HEXB
SPARC
SERINC3
CTSS
D
Human Xeno MG
Mouse microglia
z-score
E
Human Xeno MG Enriched GO Terms
immune system process
regulation of immune system process
negative regulation of biological process
negative regulation of immune system process
peptide metabolic process
leukocyte activation
cell activation
negative regulation of cellular process
positive regulation of myeloid leukocyte differentiation
regulation of leukocyte activation
regulation of cell adhesion
organonitrogen compound metabolic process
regulation of cell activation
cytoplasmic translation
peptide biosynthetic process
regulation of lymphocyte activation
regulation of leukocyte proliferation
positive regulation of leukocyte differentiation
cell death
positive regulation of hemopoiesis
-log10(P)
F
Human Xeno microglia
Mouse microglia
AD risk genes
log2(counts + 1)
APOC1
SORL1
MPZL1
SCIMP
MTHFD1L
HS3ST1
POLN
ECHDC3
TRIP4
CNTNAP2
ABCA7
PPP1R3B
TREML2
APOE
G
PD risk genes
log2(counts + 1)
VPS13C
SNCA
FGF20
MMRN1
LRRK2
GPNMB
GAK
SLC2A13
GCH1
MCCC1
SREBF1
SFXN2
ZFP64
PLEKHN1
CNKSR3
MANEA
RAI1
GBA
SCARB2
SYT11
H
AD risk genes
same trend
4
10
4
chimeric brain
Gosselin et. al.,2017
PD risk genes
same trend
2
18
2
chimeric brain
Gosselin et. al.,2017